Slider-Bearing Design with Micro-Machined Wavy-Cavity : Parametric Characterization of Thermohydrodynamic-Operation-Scheme

B. Turker Ozalp

Department of Industrial Engineering, Uludag University,
16059 Gorukle Bursa, Turkey

A. Alper Ozalp*

Department of Mechanical Engineering, Uludag University,
16059 Gorukle Bursa, Turkey

Slider bearings are widely applied in mechanical systems, where the design needs cover increased load capacity, lowered friction and power consumption and creative designs. This work is governed to perform a parametric characterization, by generating a novel structure on the upper slider surface, which can formally be expressed in micro-machined wavy-form, where the individual and combined influences of various structural design parameters and boundary conditions, on the performance records, are also evaluated. Computations put forward that the contribution of the wave amplitude on power loss values is highly dependent on the level of inlet pressure ; higher amplitudes are determined to increase power loss in the lowest inlet pressure case of 1.01, whereas the contrary outcome is determined in the higher inlet pressure cases of 3.01 & 5.01. Designing the slider bearing system, based on optimal load capacity, produced the optimum wave number ranges as 10-45, 7-11 and 5-8 for the pad inclinations of 5°, 4° and 3° respectively.

Nomenclature

C_p	: Constant pressure specific heat, J/kgK
F_f	: Friction force, N
h	: Bearing height, m
k, b, ζ	: Viscosity parameters
L	: Bearing length, m
n	: Number of sequential cells
$\dot{m}$	: Lubricant flow rate, kg/s
P	: Static pressure, Pa
q_x	: Volumetric flow rate per unit width, m³/ms

T	: Temperature, K
u	: Flow velocity, m/s
V	: Surface velocities of bearing, m/s
W	: Load carrying capacity, N
x, y	: Cartesian coordinates, m

Greek Symbols

β	: Inlet to exit pressure ratio
Δ	: Rise
ε	: Error, %
φ	: Wave amplitude, μm
$\gamma, \bar{\omega}$	: Coefficient matrices
λ	: Wave number
μ	: Dynamic viscosity, Pas
θ	: Mean pad inclination, degree
ρ	: Density, kg/m³
τ	: Shear stress, Pa
Ω_{loss}	: Power loss, W

* Corresponding Author,
  E-mail : aozalp@uludag.edu.tr
  TEL/FAX : +90-224-442-88-99
  Department of Mechanical Engineering, Uludag University, 16059 Gorukle Bursa, Turkey. (Manuscript **Received** January 12, 2006; **Revised** August 18, 2006)

Superscripts

*   : non–dimensional

Subscripts

abs,rel : Absolute, relative
cr   : Critical
i   : Node number
in, ex : Inlet, exit
l, u   : Lower–upper surfaces

1. Introduction

Bearings are employed in many industries, including hydraulic machinery, automotive and aerospace ; as the applications become extensive, investigations associated with their computer aided design/modeling (Ozalp and Ozel, 2003) and performance optimization gain higher importance, where the associated lubrication mechanism is essential for the design of sliding components. Being the power transmission element, bearings are employed in a wide range of mechanical systems ; as Cho et al.(2001) theoretically investigated the lubrication characteristics of a rotary compressor used for refrigeration and air–conditioning systems, axial hydraulic piston pumps where studied by Kim et al.(2005) and Jeong and Kim (2004), who inspected the lubricant film thickness and piston friction respectively. Magnetic (Na, 2005) and air (Yoon et al., 2002) bearings are also considered from the point of both design and performance, whereas the significance of the lubrication mechanism in the machining processes (Jun, 2005) and the role of the non–Newtonian behavior (Nouri et al., 1993) were examined as well.

Influences of various boundary and geometric conditions on the operation performances of industrial bearing systems have also been investigated both numerically and experimentally. Honchi et al.(2003) applied a micro–waviness model to an air slider bearing and van Ostayen et al.(2004) investigated the performance of a hydro–support with random waviness. The contribution of waviness on a cylindrical sliding element was considered by Rasheed (1998), who proposed a critical wave number range of 1-9 for improved operat-

ing conditions. Kwan and Post (2000) evaluated augmented load values of aerostatic bearings with higher wave amplitudes, whereas Ai et al.(1998) showed that the lubricant film thickness decreased with waviness in journal bearings. The numerical model for journal bearing systems of Liu et al. (2004) did not converge efficiently for waviness amplitudes above 6 μm ; Mehenny and Taylor (2000) also studied journal bearings and found out that the maximum pressure increased with wave number. As Su and Lie (2001) and Wong et al.(1997) numerically evaluated the effects of input pressures on the work and friction characteristics, lubricant flow rate for thrust bearing applications was handled both numerically and experimentally by Luong et al.(2004). Instabilities, based on pressure perturbations and geometric definitions, were investigated by Czolczynski (1997), on the other hand Hargreaves and Elgezawy (1998) worked on the upper surface discontinuities, and so occurring pressure variations, in slider bearings. Watanabe et al.(2000) predicted the influences structural design features on the frictional characteristics of microgrooved bearings, whereas variations of load carrying capacity with cavity geometry and surface roughness were inspected by Lin (2001) and Karkoub and Elkamel (1997) and Naduvinamani et al.(2003). A numerical model, that takes the sources of nonlinearities, such as surface waviness, into account for ball bearing applications, was developed by Harsha et al.(2003) ; additionally Sottomayor et al.(1997) studied roller bearings for various waviness amplitude values and recorded augmented friction coefficients at higher amplitude cases. Stokes and Symmons (1996) performed a multi–dimensional optimization on the plasto–hydrodynamic drawing of wires ; on the other hand the effects of various geometrical factors, such as pad length–to–width ratio, on the lubricant temperature values and power loss data of fixed–pad thrust bearings were experimentally investigated by Storteig and White (1999). Although the temperature dependent character of lubricant viscosity is well known (Shigley, 1986 ; Cameron, 1981), the numerical studies presented above disregarded this fact, due to the complexity of the numerical structure, and performed their

computations with the isotropic method, using a
fixed viscosity value in the complete flow domain.
Although fewer than the isotropic method inves-
tigations, there exist also studies that took the
viscosity variations with temperature while eval-
uating the performance of bearings. Kumar et al.
(2001) numerically investigated the heat conduc-
tion to the stationary lower surface of a linearly
narrowing slider bearing, where the temperature
dependency of lubricant viscosity was handled by
imposing the temperature distribution of the pre-
vious solution set on the current nodal viscosity
values, until the convergence criterion of 0.05%
was fulfilled among the two successive iterative
nodal temperature distributions. Pandey and Ghosh
(1998) applied the similar approach to sliding
and rolling contacts with a less sensitive conver-
gence of 0.1%, but they used a unique viscosity
value, corresponding to the average lubricant tem-
perature, in the complete flow volume. The most
precise convergence criterion (0.001%), available
in the literature, was employed by Yoo and Kim
(1997); however, to decrease the computation run
time, they did not apply the convergence to each
individual temperature value in the flow direc-
tion, but to the sum of the complete temperature
set.

In this paper we aim to characterize the ther-
modynamic operation scheme of slider bearings
parametrically, by proposing a novel structural
design, without varying the volume and the phys-
ical limits of the flow cavity, which can formally
be expressed by a micro-machined wavy-form on
the upper slider surface, where the temperature de-
pendent lubricant viscosity is also considered pre-
cisely. To produce a complete overview, compu-
tations are performed with sufficiently wide ranges
of inlet to exit pressure ratios (β), wave ampli-
tudes (φ), wave numbers (λ) and mean pad in-
clinations (θ). Performance investigations are dis-
cussed through the variations of lubricant flow
rate $(\dot{m})$, lubricant temperature rise (ΔT), power
loss (Ω_{loss}) and load carrying capacity (W) for
various β, φ, λ and θ cases; the results are dis-
played in non-dimensional form $(^*)$, so that the
findings can be applicable for various industrial
applications.

2. Methodology

2.1 Theoretical background

Plane slider bearing performance analysis cov-
ers the investigation of both momentum and en-
ergy transfer in the flow volume, thus velocity
(u), pressure (P) and temperature (T) distri-
butions are the primary concern of the funda-
mental theory. The outputs of the continuity, mo-
mentum and energy equations can be the focused
items of the work, but generally the results of the
former in the calculation order generates the input
set for the following, which puts forth the simul-
taneous handling of the three equations. As the
momentum equation in $-x$ direction (Eq. (1a))
interprets the relation of viscous shear stress and
the thermodynamic pressure, according to Shigley
(1986) the Reynolds equation for 1-dimensional
lubricant flows of slider bearings is given by
Eq. (1b), where V_u-V_l and h stand for the up-
per- lower surface velocities and pad height re-
spectively.

$$\frac{d^2u}{dy^2} = \frac{1}{\mu} \cdot \frac{dP}{dx} \qquad (1a)$$

$$\frac{d}{dx}\left(\frac{h^3}{12\,\mu}\,\frac{dP}{dx}\right) = \left(\frac{V_u + V_l}{2}\right)\frac{dh}{dx} \qquad (1b)$$

The amount of energy transferred within the lu-
bricant flow is mainly designated by the stream-
wise temperature variation but the volumetric
flow rate (q_x), the terms related to the momentum
loss and the friction loss, which is interconnected
with the shear stress (τ), lubricant density (ρ)
and specific heat (C_p), are also encountered in
Eq. (2a). Lubricant viscosity (μ) appears in either
of the 3-main flow and energy equations, thus
the Newtonian viscosity-temperature relation is
characterised by Vogel's rule (Cameron, 1981) of
Eq. (2b), where b, k and ζ are the viscosity para-
meters.

$$\rho C_p q_x \frac{dT}{dx} = V_u \tau_u + V_l \tau_l - q_x \frac{dP}{dx} \qquad (2a)$$

$$\mu = \rho k e^{\frac{b}{T+\zeta}} \qquad (2b)$$

Although the general form of the momentum, Reynolds and energy equations are as given above, calculations on slider bearing lubrication are frequently performed in non-dimensional form (Lin, 2001 ; Kumar et al., 2001 ; Hwang et al., 1996). According to Hwang et al.(1996), Eqs. (1)-(2a) can be converted into Eqs. (3)-(5) by using the non-dimensional parameters given in the Appendix, with the relevant boundary conditions.

$$\frac{d^2u^*}{dy^{*2}}=\frac{dP^*}{dx^*}$$

$$y^*=0 \rightarrow u^*=1 \text{ and} \quad (3)$$

$$y^*=\frac{h}{h_{ex}}=h^* \rightarrow u^*=\frac{V_u}{V_l}=V_u^*$$

$$\frac{d}{dx^*}\left(h^{*3}\frac{dP^*}{dx}\right)=6(V_u^*+1)\frac{dh^*}{dx^*} \quad (4)$$

$$x^*=0 \rightarrow P^*=P_{in}^* \text{ and } x^*=1 \rightarrow P^*=P_{ex}^*$$

$$q_x^*\frac{dT^*}{dx^*}=V_u^*\tau_u^*+\tau_l^*-q_x^*\frac{dP^*}{dx^*} \quad (5)$$

$$x^*=0 \rightarrow T^*=T_{in}^*$$

The non-dimensional velocity profile (Eq. (6)) can be obtained by imposing the boundary conditions in Eq. (3).

$$u^*=\frac{dP^*}{dx^*}\frac{y^*}{2}(y^*-h^*)+(V_u^*-1)\frac{y^*}{h^*}+1 \quad (6)$$

Integration of the velocity profile gives the lubricant flow rate per unit width (Eq. (7)).

$$\dot{m}^*=\int_0^{h^*}u^*dy^*=\frac{-1}{12}\frac{dP^*}{dx^*}h^*+(V_u^*+1)\frac{h^*}{2} \quad (7)$$

The streamwise pressure distribution can be evaluated by integrating the Reynolds equation twice,

$$P^*=\int_0^{x^*}\frac{\int 6(V_u^*+1)dh^*}{h^{*3}}dx^*-c_1\int_0^{x^*}\frac{dx^*}{h^{*3}}+P_{in}^* \quad (8)$$

where the integration constant c_1 can be determined by using a manometric pressure boundary condition : $P^*(x^*=1)=0$, together with the 2 new functions of $f(h^*)$ and $g(h^*)$ as given below :

$$C_1=\frac{\int_0^1 g(h^*)dx^*}{\int_0^1 f(h^*)dx^*} \quad (9a)$$

$$g(h^*)=\frac{\int 6(V_u^*+1)dh^*}{h^{*3}} \quad (9b)$$

$$f(h^*)=\frac{1}{h^{*3}} \quad (9c)$$

In addition to the inlet conditions and surface velocities, especially the streamwise pressure gradient (dP/dx) and the shear stress values at the upper (τ_u) and lower (τ_l) surfaces (Eqs. (10a)-(10b)) also participate as inputs when the temperature variation is under inspection. Superimposing the finite difference sense into the energy equation and rearranging the terms of Eq. (5) brings up a thermal relation (Eq. (11)) within two consecutive nodes in the flow domain, which in return displays the lubricant temperature distribution in the flow direction.

$$\tau_u^*=\frac{dP^*}{dx^*}\frac{h^*}{2}+\frac{V_u^*-1}{h^*} \quad (10a)$$

$$\tau_l^*=-\frac{h^*}{2}+\frac{V_u^*-1}{h^*} \quad (10b)$$

$$T_{i+1}^*=T_i^*+\left[\frac{V_u^*\tau_u^*+\tau_l^*}{\frac{-1}{12}\frac{dP^*}{dx^*}h^*+(V_u^*+1)\frac{h^*}{2}}-\frac{dP^*}{dx^*}\right]_i\Delta x^* \quad (11)$$

The overall lubricant temperature rise in the flow volume can be evaluated by the sigma notation of Eq. (12), which is based on the cellular (n) temperature augmentations in the flow domain. The load-carrying capacity (W^*) is obtained by the streamwise integration of the film pressure and the power loss (Ω_{loss}^*) value is evaluated by the direct multiplication of the lubricant flow rate and the lubricant temperature rise data. Expressing in terms of dimensionless quantities yields Eqs. (13)-(14).

$$\Delta T^*=\sum_{i=1}^n\left[\frac{V_u^*\tau_u^*+\tau_l^*}{\frac{-1}{12}\frac{dP^*}{dx^*}h^*+(V_u^*+1)\frac{h^*}{2}}-\frac{dP^*}{dx^*}\right]_i\Delta x^* \quad (12)$$

$$W^* = \int_0^1 \left[\int_0^{x^*} \frac{\int 6(V_u^*+1)\,dh^*}{h^{*3}}\,dx^* - c_1 \int_0^{x^*} \frac{dx^*}{h^{*3}} + P_{in} \right] dx^* \quad (13)$$

$$\Omega_{loss}^* = \dot{m}^* \Delta T^* \quad (14)$$

2.2 Computational method

The computational procedure is carried out on the geometric domain of Fig. 1(a), by dividing the flow volume into n sequential cells. Numerical investigations are performed by the simultaneous solution of the continuity, momentum and energy equations; however the wavy-form of the upper surface is determined to cause singularities, and so occurring converging problems, in the mesh, particularly in the neighborhoods of the crest and base points. To overcome the difficulties, based on the locally intense variations of cavi-
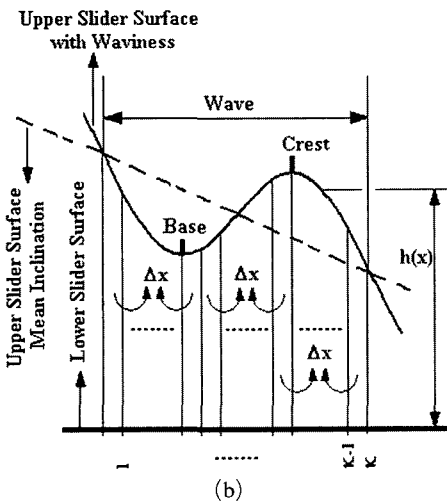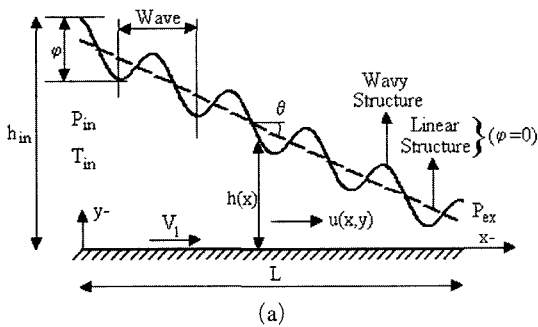

(a)

(b)

Fig. 1 (a) Schematic layout of slider bearing with/without micro-machined wavy structure at the upper surface, (b) Meshing strategy within the wavy cavity

ty height and lubricant viscosity values in the streamwise direction, mesh density (n) is varied in accordance, so that each crest and base point is assigned a node, which makes it possible to take the extreme gradients in all of the flow parameters into account. The flow domain is modeled with a constant cell width of $\Delta x \ (=L/n)$ in the streamwise direction and the incompressible lubricant flow is simulated with 2nd order finite difference marching procedure (Chapra and Canale, 1990).

The relation of geometric structure, static pressure and velocity distributions in the flow cavity is presented by equating the derivative of the lubricant flow rate $(\dot{m}^*)$ formula of Eq. (7) to zero, which as a consequence forms a system of $n-1$ linear equations. The system of linear equations can be designated in closed form via sigma notation by Eq. (15), or in explicit form by Eq. (16) interpreting the interactions of the neighboring nodes in the mesh. Eqs. (15)-(16) involve left hand side coefficients $(\gamma_{i=1,\cdots,n+1})$ and right hand side values $(\bar{\omega}_{i=1,\cdots,n+1})$, whose elements are mainly defined by the groove geometry and the upper and lower surface velocities of the bearing and can be calculated in matrix form by Eqs. (17)-(18) respectively. The explicit form of the $n-1$ equations constitute the "Transfer Matrix" (Eq. (16)) of the system; since the nodes $i=1$ and $i=n+1$ represent the inlet and exit planes, the flow (u, P, T) and lubricant (μ) parameters of the in-between nodes from $i=2$ to n are the scope of continuity and Reynolds equations.

$$\sum \gamma_i P_i^* = \bar{\omega}_i \quad (15)$$

$$i=1 \qquad \rightarrow \gamma_{i+1} P_{i+1}^* + \gamma_{i+2} P_{i+2}^* = \bar{\omega}_i - \gamma_i P_{in}^*$$

$$1 < i < n-1 \rightarrow \gamma_i P_i^* + \gamma_{i+1} P_{i+1}^* + \gamma_{i+2} P_{i+2}^* = \bar{\omega}_i \quad (16)$$

$$i=n-1 \quad \rightarrow \gamma_i P_i^* + \gamma_{i+1} P_{i+1}^* = \bar{\omega}_i - \gamma_{i+2} P_{ex}^*$$

The elements of the transfer matrix, given by Eq. (16), are defined by 2 single-row sub-matrices $(\gamma_{i=1,\cdots,n+1}, \ \bar{\omega}_{i=1,\cdots,n+1})$, whose elements can be computed as follows,

$$\gamma_i = h_i^{*3} \quad (17a)$$

$$\gamma_{i+1} = -[h_i^{*3} + h_{i+1}^{*3}] \quad (17b)$$

$$\gamma_{i+2} = h_{i+1}^{*3} \quad (17c)$$

$$\bar{\omega}_i = 6 \, (V_u^* + 1) \, \Delta x^* \, (h_{i+1}^* - h_i^*) \qquad (18)$$

where i defines the successive node numbers in the streamwise direction.

Although the traditional isotropic method, which ignores the temperature dependent character of lubricant viscosity, is still applied in many studies, due to the significant role of viscosity variation on the performance data (Ozalp and Ozel, 2003 ; Kumar et al., 2001 ; Pandey and Ghosh, 1998 ; Yoo and Kim, 1997), the computations of the present study are operated with the iterative transfer matrix approach, where the solution of the traditional isotropic method is considered as the initial set of guesses for the next iteration step. The temperature distribution of the isotropic approach is used in the next step of the iterative method to evaluate the nodal viscosity variation by Eq. (2b) with the viscosity parameters of k, b, ζ. Solving the transfer matrix of Eq. (16), with the so obtained viscosity distribution, gives the stepwise temperature set of the iterative method. The computations are performed until two consecutive temperature distributions are not more than 0.01% distant, being more sensitive than that of Pandey and Ghosh (1998) (0.1%) and Kumar et al.(2001) (0.05%), at each node within the mesh. Although Yoo and Kim (1997)'s criterion (0.001%) on the sum of the complete temperature set appears to be more precise, imposing the convergence on each nodal temperature in the present method results in $n+1$ times more control loops for every iteration step, which brings about considerably more reliable temperature records.

2.3   Meshing and convergence

Authors developed a solver computer program to handle the Reynolds (Eq. (16)) and energy (Eq. (11)) equations by evaluating the single-row sub-matrix elements of $\gamma_{i=1,\cdots,n+1}$ & $\bar{\omega}_{i=1,\cdots,n+1}$ (Eqs. (17)-(18)) for each node in the mesh. As thermal and hydrodynamic flow-field variables are to be calculated at the nodes from $i=1$ to $i=n+1$, regarding the direction of the lower slider surface movement, thus lubricant flow, the cavity between the inlet and exit sections is divided into a finite number of cells where the basic

idea is to generate a systematic meshing by also considering the locations of the crest and base points of the wavy upper slider surface. Since the task is to sensitively express the control volume terms using the grid point values, several preliminary computational runs are performed with various meshing styles to investigate the grid dependence of the solution. To overcome the problems on discontinuities, due to the wavy pattern, each crest and base point is assigned a node. The in-between nodes of each wave on the surface are positioned with the definition of wave cell number (κ) which satisfies the condition that the numerical outputs are independent of the meshing employed. The wave cell number range is selected as $\kappa = 10 \rightarrow 200$ depending on the number of waves $(\lambda = 105 \rightarrow 5)$ employed on the upper surface. As a consequence, the total cell number is determined with constant cell width (Δx) selection and homogeneous distribution style, which results in the total cell number range as $n = 950-1050$, and the scheme is given in Fig. 1(b). Such as, for the cases of $\lambda = 5, 45, 95$ and 105, the κ values are fixed to $200, 22, 10$ and 10, resulting in the n data of $1000, 990, 950$ and 1050 respectively. Increasing the meshing density beyond these limits pointed out no change in the nodal property evaluations, which verifies the sufficiently stable character of discretization with $950 \leq n \leq 1050$. The solution algorithm involves 3 subroutines : the first satisfies the Reynolds equation (Eq. (16)) with the computation of the single-row sub-matrices (Eqs. (17)-(18)) ; second subroutine evaluates the energy transfer rate (Eq. (11)) in the flow direction and the third checks the uniqueness of the nodal results (P, T, μ, u) by comparing the very last 2 iteration step nodal-temperature values in the flow domain. The basic idea is to update the temperature (thus viscosity) distribution, by applying mass flux conservation, satisfying thermal equilibrium at each pressure boundary within the mesh, such that the mass flow rate conserves and the simulated boundary pressures coincide with the imposed values at the inlet and exit planes. The iteration procedure is repeated until convergence of the nodal temperature (T_i) results is achieved with a relative error
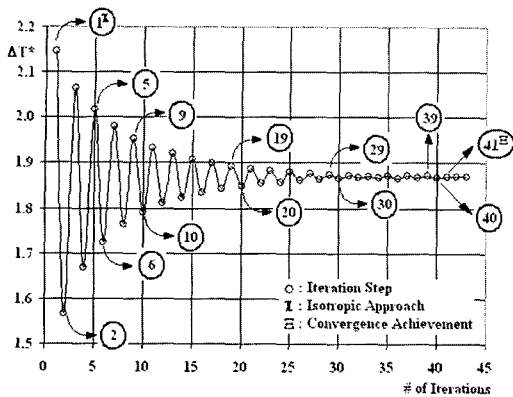
Fig. 2 Graphical iterative convergence-outline of the lubricant temperature rise data of a specific slider bearing configuration

of $\varepsilon_{rel}=0.01\%$ at the j-th iteration step, i.e.

$$\max\left(\frac{|T_i^j-T_i^{j-1}|}{T_i^j}\right)*100\le\varepsilon_{rel} \qquad (19)$$

for $i=1,2,\cdots,n+1$, where j represents the current iteration step number in the solution algorithm.

As an illustrative example, on the computational convergence phenomena of inclined slider bearing lubrication process with micro-machined wavy-cavity, the specific case with $\beta=5.01$, $\lambda=5°$, $\lambda=105$ and $\varphi=200$ μm is selected. Since the definition of lubricant temperature rise is given as $\Delta T^*=T_{n+1}^*-T_1^*$, the graphical presentation of the iterative convergence-outline is based on ΔT^* and shown in Fig. 2 and also in Table 1(a) based on relative error (ε_{rel}).

The first iteration step stands for the isotropic case (χ) with constant viscosity, whereas the subsequent steps are carried out with the previous temperature distribution. The convergence of the lubricant temperature rise value to $\Delta T^*=1.866$ is achieved at the 41st iteration (E) for this particular run and the decay of ε_{rel} for ΔT^* is also evident in Table 1(a) where the relative error among the 40th-41st iteration steps is 0.008% (Table 1 (a)), being less than the applied convergence criterion of 0.01%. Moreover, Fig. 2 and Table 1(a) simultaneously point out the fact that ΔT^* data do not vary if the numerical iterations are further executed (i.e. $j=42$, 43, $\cdots$).

Table 1 Tabulated iterative convergence-outline of the slider bearing performance data based on (a) Relative error (ε_{rel}) and (b) Absolute error (ε_{abs})

(a)

Iteration # j	Relative Error (ε_{rel})			
	ΔT^*	$\dot{m}^*$	Ω_{loss}^*	W^*
2	37.02	1.71	13.45	6.50
5	24.15	36.47	20.51	16.48
6	16.97	2.14	9.06	4.94
9	12.97	8.66	10.25	7.37
10	9.02	1.67	5.59	3.18
19	7.31	3.37	5.52	3.71
20	2.31	0.59	1.60	0.94
29	1.93	0.62	1.40	0.89
30	0.49	0.14	0.34	0.22
39	0.38	0.07	0.31	0.18
40	0.20	0.02	0.18	0.10
41^E	0.008	0.009	0.011	0.006
42	0.000	0.000	0.000	0.000

E : Iteration $j=41$ stands for convergence achievement

(b)

Iteration # j	Relative Error (ε_{rel})			
	ΔT^*	$\dot{m}^*$	Ω_{loss}^*	W^*
1$^\chi$	14.79	1.23	10.91	6.72
2	16.22	21.13	11.39	8.22
5	7.82	1.18	5.61	3.46
6	7.82	5.00	5.28	3.54
9	4.43	0.85	3.22	1.95
10	4.21	1.95	2.85	1.83
19	1.17	0.26	0.89	0.52
20	1.11	0.41	0.74	0.47
29	0.22	0.03	0.25	0.13
30	0.27	0.18	0.09	0.09
39	0.09	0.02	0.07	0.04
40	0.10	0.01	0.11	0.06
41^E	0.00	0.00	0.00	0.00

χ : Iteration $j=1$ stands for the constant viscosity isotropic approach

Table 1(a) additionally illustrates not only the dependence of the other performance parameters,

like lubricant flow rate $(\dot{m}^*)$, power loss (Ω_{loss}^*) and load carrying capacity (W^*), on ΔT^* but also their convergence history to the actual data at the iteration step of $41^Ξ$.

$$\varepsilon_{abs} = \left(\frac{|\pi^Ξ - \pi^j|}{\pi^Ξ}\right) * 100 \qquad (20)$$

On the other hand, although the role of viscosity variation with temperature on the operation characteristics is apparent both in Fig. 2 and Table 1(a), with the additional definition of absolute error (Eq. (20)) the shift of the performance parameter (π) data at any iteration step from the actual values $(Ξ)$ can be evaluated, where ε_{abs} values are given in Table 1(b) for certain iteration steps. The tabulated values put forward that the constant viscosity consideration (χ) creates the highest error in ΔT^* with 14.79% whereas the corresponding ε_{abs} for Ω_{loss}^*, W^* and $\dot{m}^*$ are 10.91%, 6.72% and 1.23% respectively ; the decay of absolute error, especially after the second iteration $(j=2)$, is evident for all parameters.

The presented graphical (Fig. 2) and tabulated (Table 1) iterative convergence-outline of the specific case clearly puts forward not only the stable discretization of the employed meshing method but also the reliable character of the performed computations with the relatively sensitive convergence criterion, which as a whole sufficiently justify the accuracy of the numerical evaluations that are documented in the Results and Discussion section of the article.

2.4 Model slider bearing

To produce an adoptable slider bearing model for real time industrial applications, the necessary physical and the thermo-fluid compounds are assembled from the available recent numerical studies. Computations are performed with SAE 20 type lubricant that has comparable viscosity values of Mehenny and Taylor (2000)'s application, and with the inlet temperature (T_{in}) of 20℃, which is close to that of Sottomayor et al.(1997) (24℃). Inlet (P_{in}) and exit (P_{ex}) oil pressure values are decided to be 101-501 kPa (with 25 kPa increments) and 100 kPa respectively, which propose the β (Eq.(21a)) range of 1.01-5.01. Bearing

length (L) is selected as 10 mm, being between the choices of Honchi et al.(2003) (1.25 mm) and Ai et al.(1998) (14.5 mm). As the inlet height (h_{in}) is fixed to 1 mm, the exit height (h_{ex}) range is selected as 0.475-0.125 mm, where these values are within the most frequently applied bearing pad height and journal bearing clearance data range of 1-0.0175 mm (Lin, 2001 ; Liu et al., 2004). The employed inlet and exit heights result in the h_{in}/h_{ex} ratio range of 2.1-8 and the mean pad inclination range (θ) of 3°-5° (Fig. 1(a)). As the resulting h_{in}/h_{ex} ratio range is compatible with those of Das (1998) and Kumar et al.(2001), where the upper limit of their corresponding h_{in}/h_{ex} ratio ranges were 6 and 10 respectively, the consequential pad inclination (Eq.(21b)) range also suits with the applied values of Watanabe et al.(2000) $(\theta=1.78°)$, Honchi et al.(2003) $(\theta=6.8°)$ and Dadouche et al.(2000) $(\theta=12°)$.

$$\beta = \frac{P_{in}}{P_{ex}} \qquad (21a)$$

$$\theta = \tan^{-1}\left(\frac{h_{in}-h_{ex}}{L}\right) \qquad (21b)$$

The lower surface is assigned a velocity of $V_l=5$ m/s, which is the mean value of the corresponding data of Liu et al.(2004) (2.55-10.21 m/s) and of Ai et al.(1998) (8.79 m/s), whereas the upper bearing surface is kept stationary $(V_u=0$ m/s) as in the study of Honchi et al.(2003). Similar to that of van Ostayen et al.(2004) and Kwan and Post (2000), the general scheme of the slider bearing under consideration here is narrowing in linear style (Fig. 1(a)) ; moreover to investigate the influences of the wavy pattern on the upper surface, wave amplitude (φ) and wave number (λ) are contributed in sufficiently wide ranges of $\varphi=0-200$ μm, covering those of Harsha et al. (2003), Rasheed (1998) and Liu et al.(2004), and $\lambda=5-105$, similar those of Honchi et al. (2003), Kwan and Post (2000) and Sottomayor et al.(1997). To fit conveniently the main consideration of the present parametric study, the cosine curve of Eq.(22) is implemented to the streamwise-structure of the upper slider surface, where the number of waves, the wave amplitude,

Table 2 Model slider bearing data

Parameter	Symbol	Range	Increment
Pad Style	—	Linear	—
Lubricant	—	SAE 20*	—
Upper Surface Velocity	V_u	0 m/s	—
Lower Surface Velocity	V_l	5 m/s	—
Bearing Length	L	10 mm	—
Pan Inlet Height	h_{in}	1 mm	—
Mean Pad Inclination	θ	3°-5°	0.01°
Inlet Temperature	T_{in}	20°C	—
Inlet Pressure	P_{in}	101-501 kPa	25 kPa
Exit Pressure	P_{ex}	100 kpa	—
Pressure Ratio	β	1.01-501	0.25
Wave Amplitude	φ	0-200 μm	40 μm
Wave Number	λ	5-105	10

*(ρ=861 kg/m³, k=0.110223 m²/s, b=679.713 K, ζ=69.3176 K)
*Shighey, 1986

the relative position of nodes and the total mesh-ing scale are indicated by λ, φ, i and $n+1$ re-spectively. The overall model slider bearing data is given in Table 2.

$$h(x) = h_{in} - x \tan \theta + \frac{\varphi}{2} \left[\cos \left(2\pi \frac{i}{n+1} \lambda \right) \right] \quad (22)$$

3. Results and Discussion

Numerical investigations are performed with wave numbers (λ) of 5-105, wave amplitude (φ) values are in the range of 0-200 μm, slider bear-ing mean pad inclination (θ) is varied between 3°-5° and the inlet pressures are 1.01-5.01 times (β) the exit value. Results of various structural-design and boundary condition cases are discuss-ed through the non-dimensional values of lubri-cant flow rate ($\dot{m}^*$), lubricant temperature rise (ΔT^*), power loss (Ω_{loss}^*) and load carrying ca-pacity (W^*).

3.1 Lubricant flow rate ($\dot{m}^*$)

Lubricant flow rate ($\dot{m}^*$) variations with wave number (λ) and pad inclination (θ), considering also a variety of wave amplitude (φ) and inlet pressure (β) conditions, are demonstrated in Figs.

3(a)-(b) respectively. For the inlet condition of β=1.01 (Fig. 3(a)) computations indicate, for the lower wave amplitude range of 0-80 μm (φ_1-φ_3), a linear relationship between lubricant flow rate and pad inclination (3°≤θ≤5°) with 5≤λ≤25; however for higher wave amplitudes (φ_4=120 μm-φ_6=200 μm) the linear dependence is valid only in a narrower pad inclination range of 3°-3.77°, where the upper pad inclination limit comes out to be critical and can be designated by θ_{cr}. On the other hand, the wavy structures on the upper surface with φ≥120 μm produce the counter effect on lubricant flow rate and the out-comes become more notable in the cases with higher φ, λ and θ. Moreover, for cavities with low θ and λ does not create variations in $\dot{m}^*$, but above the critical pad inclination (θ_{cr}=3.77°) lubricant flow rate decreases with higher wave numbers for the complete range of φ. Fig. 3(a) additionally puts forward that for the complete set of pad inclinations (θ=3°-5°), higher wave amplitudes result in lower lubricant flow rate; particularly above the critical inclination of θ_{cr}= 3.77° the impact of φ becomes more sensible in the wave number range of 5<λ<25.

Fig. 3(b) displays the variation of lubricant flow rate with pad inclination (θ), for various wave amplitudes (φ) and inlet pressures (β), with the maximum wave number of λ=105. As can be seen from the figure that, in the complete set of pad inclinations and wave amplitudes investigat-ed, there exists a linear relation between $\dot{m}^*$ values and β. For the lowest pad inclination case of θ= 3°, wave amplitudes do not have influence on the flow rate values in lower inlet pressure conditions (β≈1.01), where the $\dot{m}^*$ data of the φ_6=200 μm case is below that of the φ_1=0 μm surface (no-wave) by only 4.36%. However as the pad incli-nation is increased, the corresponding propor-tions become 10.64% and 61.68% for θ=4° and θ=5° respectively, which denote the augmented role of wave number on lubricant flow rate in systems with higher pad inclinations. Watanabe et al.(2000) also determined 1-1.4% augmented flow rate values with comparably smaller wavi-ness amplitudes (φ=2-6 μm) in journal bearings. Moreover, for β≥2, cavities with higher pad
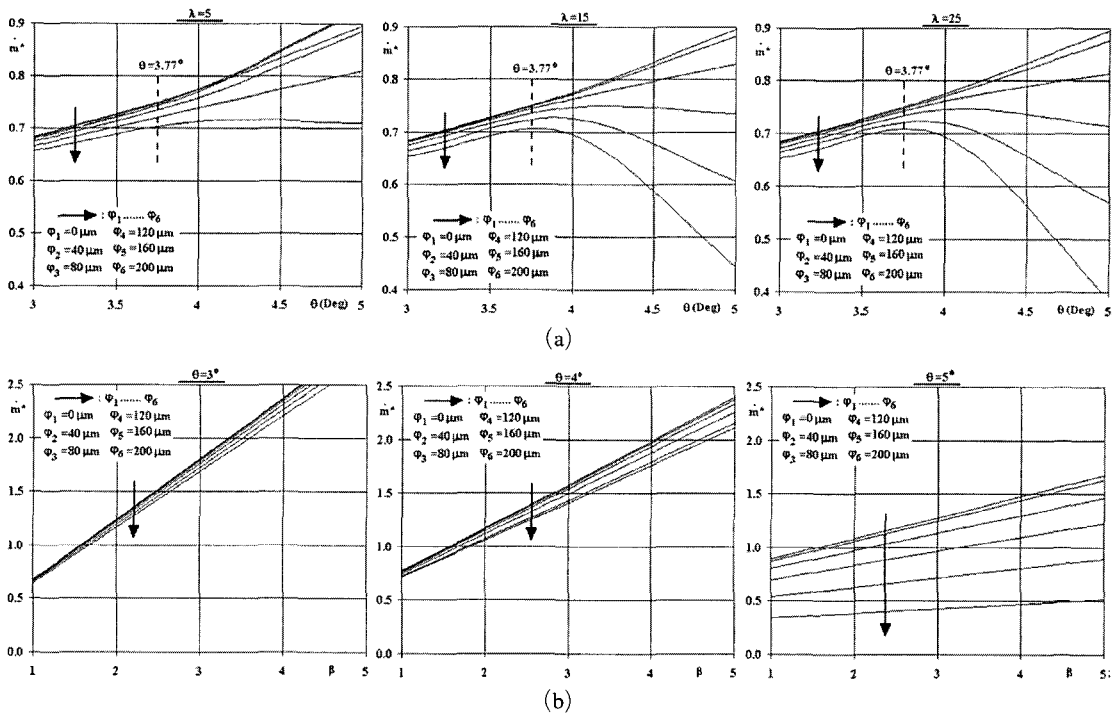
(a)

(b)

Fig. 3 Combined effects of (a) θ, φ and λ (at β=1.01) and (b) θ, φ and β (at λ=105) on lubricant flow rate

inclination result in lower lubricant flow rate values, where this outcome is similar to those of Luong et al.(2004) and Watanabe et al.(2000), who determined lower mass flow rates with lower cavity heights in aerostatic thrust bearings (Luong et al., 2004) and with diametral clearance in microgrooved journal bearings (Watanabe et al., 2000), which correspond to lower pad inclinations. It can also be seen from the figure that the family of flow rate lines are steeper in the lowest pad inclination case of θ=3° than those of the bearings with θ=4° and θ=5°. By denoting the individual influence of inlet pressure on lubricant flow rate with the partial derivative of $\partial \dot{m}^*/\partial \beta$, the slopes of the line-families are evaluated as $0.564 \rightarrow 0.521$ (θ=3°), $0.402 \rightarrow 0.334$ (θ=4°) and $0.190 \rightarrow 0.044$ (θ=5°) in the complete wave amplitude range (φ=0 → 200 μm) considered, where the slope values additionally indicate the augmented effects of β on $\dot{m}^*$ in bearings with lower φ.

3.2　Lubricant temperature rise (ΔT^*)

Lubricant temperature rise (ΔT^*) variations with pad inclination (θ), wave amplitude (φ) for

various wave number (λ) and inlet pressure (β) cases are shown in Figs. 4(a)-(b) respectively. Fig. 4(a) indicates for the specific case of β=1.01 that, the complete set of ΔT^* curves decrease linearly with pad inclination for λ=5, however the lubricant temperature rise values exhibited augmentations in designs with higher wave numbers ($\lambda \geq 15$) above the critical pad inclination (θ_{cr}) of 3.77°, especially for the wave amplitudes of 160 & 200 μm (φ_5 & φ_6), where the augmentations become more remarkable in the cases with higher φ, λ and θ. These results resemble those of Wang and Zhu (2006), who also determined lower ΔT^* values at low eccentricity cases and recorded augmented temperature rise data with the increase of eccentricity, in journal bearing applications. The curves of Fig. 4(a) additionally imply that, higher wave amplitudes cause augmented lubricant temperature rise values for the complete pad inclination range (θ=3°-5°); the impact of wave amplitude on ΔT^* becomes more evident particularly in the range of φ=120-200 μm ($\varphi_4 - \varphi_6$) for $5 \leq \lambda \leq 25$. Nevertheless, for lower pad inclination cases (θ=3°-3.5°), the

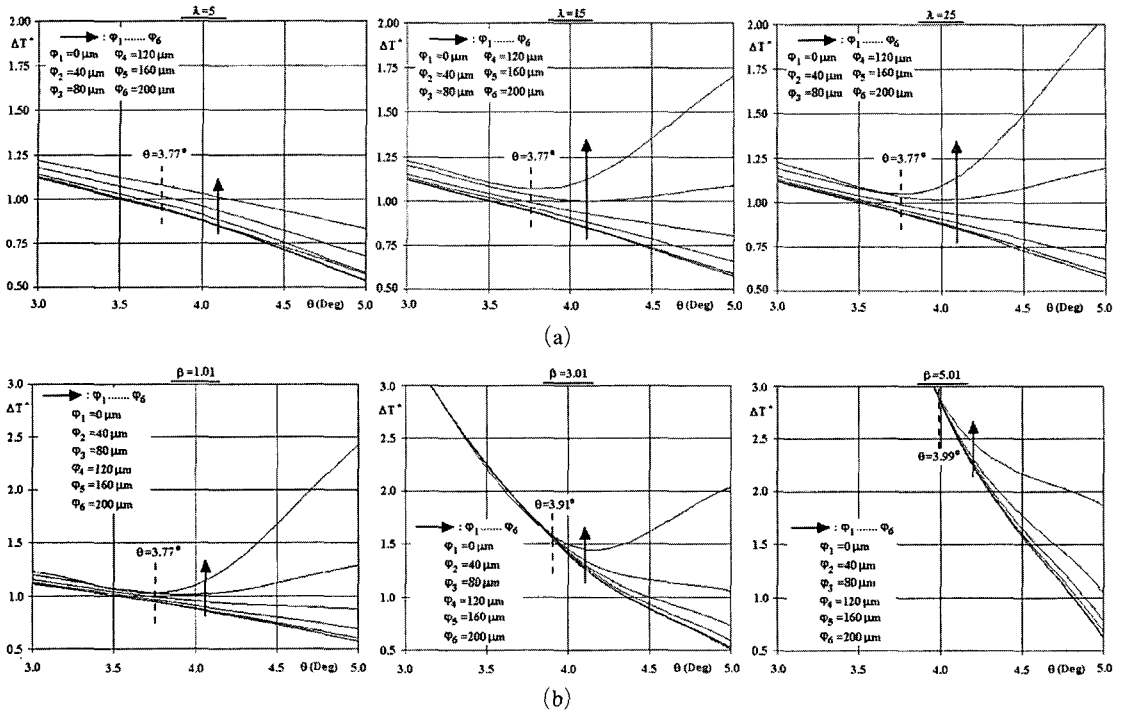**Fig. 4** Combined effects of θ and φ on lubricant temperature rise for various
(a) λ (at $\beta=1.01$) and (b) β (at $\lambda=105$) cases

temperature rise values come out not to be in-fluenced by wave number, however above $\theta_{cr}=3.77°$, especially with higher φ cases, wave num-bers cause augmentations in ΔT^* values.

Fig. 4(b) shows the variation of lubricant tem-perature rise with inlet pressure (β), by also con-sidering the combined influences of various pad styles for the complete set of φ and θ values, with the maximum wave number of $\lambda=105$. Computa-tions put forward that the role of wave ampli-tude on ΔT^* is negligible in the pad inclination ranges of $\theta<3.77°$, $\theta<3.91°$ and $\theta<3.99°$ for β of 1.01, 3.01 and 5.01 ; but for the systems with higher pad inclinations the influence becomes iden-tifiable, such as the maximum φ of 200 μm results in an increase in ΔT^* values, particularly for the $\theta=5°$ case, by 4.22, 4.03 and 3.03 folds of the $\varphi=0$ surface for β of 1.01, 3.01 and 5.01 respectively, denoting that the influence of φ on ΔT^* drops with higher β. On the other hand, the temperature rise values of the designs with $\theta=3°$ & $4°$-$\lambda=25$ (Fig. 4(a)) and $\theta=3°$ & $4°$-$\lambda=105$ (Fig. 4(b)) are relatively close, having a variation rate of less

than 0.8%, revealing the ineffective character of wave number on temperature rise values in the range of $25\leq\lambda\leq105$ for the pad inclinations of $\theta=3°$ & $4°$. However in the highest pad inclina-tion case of $\theta=5°$, the ΔT^* values are apparently effected by wave number in the range of $\lambda=25$-105, where the most significant differences are recorded at the highest wave amplitude of $\varphi=200$ μm with an increase rate of up to 19.8% in the complete β set. It can also be seen from Fig. 4(b) that, the complete set of ΔT^* curves attain higher values in the low pad inclination $(\theta\leq4°)$ and in the high inlet pressure $(\beta\geq3.01)$ cases, being independent of the level of φ, which de-notes the dominant character of pad inclination on ΔT^*, when compared to that of the wave amplitude, in the high β cases. The relation of pad structure and lubricant temperature varia-tions in fixed pad thrust bearings were also con-sidered by Storteig and White (1999), who re-corded elevated temperature rise data with higher cavity heights, which correspond to lower pad inclinations. Moreover, increasing β resulted in
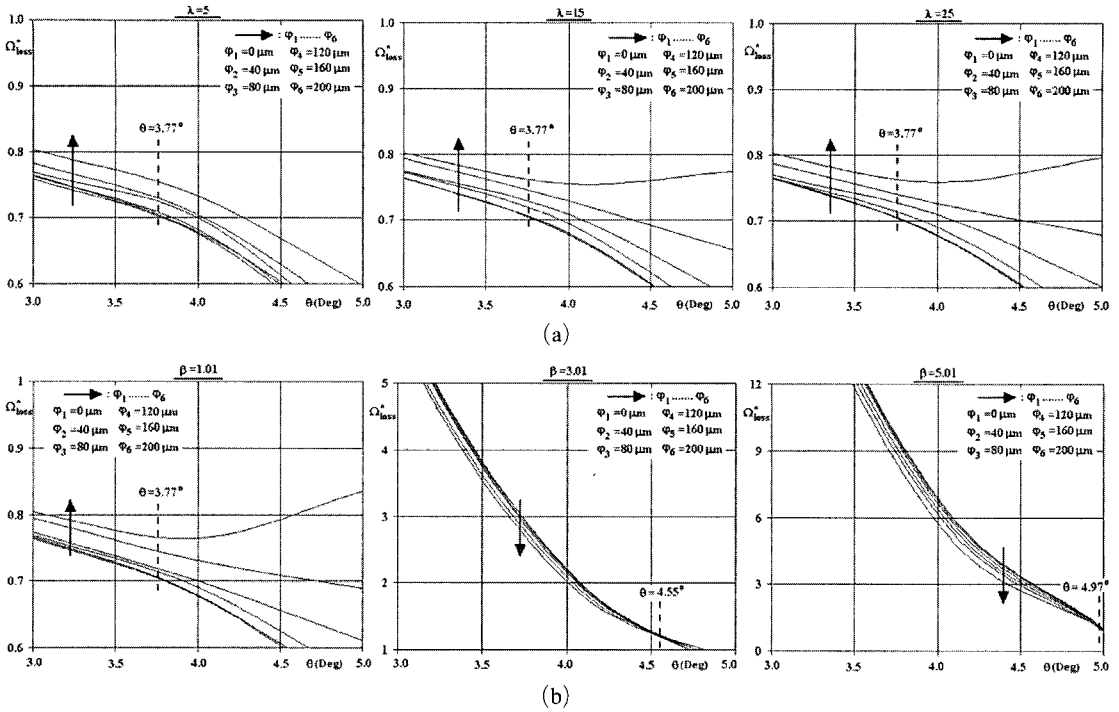
Fig. 5 Combined effects of θ and φ on bearing power loss for various
(a) λ (at $\beta = 1.01$) and (b) β (at $\lambda = 105$) cases

considerable augmentations in the lubricant temperature rise values especially in the cavities with lower inclinations ($\theta = 3° - 4.22°$), however further narrowing the lubrication structure ($\theta > 4.22°$) constitutes closer ΔT^* values among the inlet pressure cases of $\beta = 1.01$ & 5.01, with the two design exclusions of $\varphi = 160$ & 200 μm, that attain slightly lower temperature rise values at higher inlet pressures.

3.3 Bearing power loss (Ω^*_{loss})

Figure 5(a) displays the variation of power loss values with wave number (λ) for the inlet pressure case of $\beta = 1.01$. As can be seen from the figure that, implementation of higher wave numbers ($\lambda = 5 \rightarrow 25$) did not have any contribution on Ω^*_{loss} for the pad inclinations of $\theta < \theta_{cr}$ in the complete wave amplitude range ($\varphi = 0 \rightarrow 200 \mu m$). On the other hand, the slopes of the $\varphi \leq 120 \mu m$ curves increase above the critical pad inclination of $\theta_{cr} = 3.77°$; the figure additionally puts forward that the amount of slope change with θ is more notable in lower λ cases ($\lambda = 5$ & 15) which

denotes the remarkable influence of higher θ on the power loss values at low wave number cases. Although the power loss values of the $\lambda = 5$ case, for the complete wave amplitude scenarios investigated, continuously decrease with pad inclination, in the surface definitions with higher wave number ($\lambda \geq 15$) the Ω^*_{loss} values of the $\varphi = 200 \mu m$ case increase with pad inclination above the critical limit of $\theta_{cr} = 3.77°$, which implies that the specific wave amplitude of 200 μm creates synergy on the power loss values in the geometric design definitions of $\theta \geq 3.77°$ and $\lambda \geq 15$.

The variation of power loss values (Ω^*_{loss}) with inlet pressure (β) for systems with various φ and θ combinations for the specific case of $\lambda = 105$ are presented in Fig. 5(b). The curves of the plot put forward that the power loss values increase with higher inlet pressure cases, such as the augmentation rates among the $\beta = 3.01$ and $\beta = 1.01$ cases $((\Omega^*_{loss})_{\beta=3.01}/(\Omega^*_{loss})_{\beta=1.01})$ are $7.99 \rightarrow 7.17$ ($\varphi = 0 \rightarrow 200 \mu m$) for the pad inclination of $\theta = 3°$ and $1.25 \rightarrow 0.99$ ($\varphi = 0 \rightarrow 200 \mu m$) for the pad with $\theta = 5°$, where the similar ratios among the

$\beta=5.01$ and $\beta=1.01$ cases $((\Omega^*_{loss})_{\beta=5.01}/(\Omega^*_{loss})_{\beta=1.01})$ are evaluated as $28.89 \to 25.79$ and $1.99 \to 1.16$ for θ of $3°$ and $5°$ respectively. These records not only indicate that the influence of β on Ω^*_{loss} is more remarkable in systems with lower θ and φ, but also show parallelism with the discussions on lubricant flow rate variations with β through Fig. 3(b). Moreover, excluding the specific case of $\beta=1.01$-$\varphi=200$ μm, similar with the lower power loss records of Storteig and White (1999) on lower cavity heights, the pad inclination constituted the counter effect on the power loss values and resulted in lower Ω^*_{loss} for the entire β and φ set, where the impact of θ on Ω^*_{loss} becomes significant in higher β scenarios with the ratios of $((\Omega^*_{loss})_{\theta=5}/(\Omega^*_{loss})_{\theta=3})$ $0.680 \to 1.038$ ($\varphi=0 \to 200$ μm), $0.107 \to 0.142$ and $0.0462 \to 0.0467$ for β of 1.01, 3.01 and 5.01 respectively, which additionally indicate the amplified influence of θ on Ω^*_{loss} at higher wave amplitude (φ) values. Computations put forward that there exist critical pad inclinations (θ_{cr}), where the power loss variations show apparent deviations both from the point of style and slope. Similar to those of Fig. 5(a), the slopes of the $\varphi \le 120$ μm curves ($\beta=1.01$) increase above the critical pad inclination of $\theta_{cr}=3.77°$, whereas the power loss values of the surface definition with $\varphi=200$ μm show augmentation beyond the same inclination, which was also determined for the wave number range of $\lambda \ge 15$ in Fig. 5(a). As the inlet pressure is increased to $\beta=3.01$ and 5.01 power loss values are determined to coincide at the pad inclinations of $\theta_{cr}=4.55°$ and $4.97°$ respectively. On the other hand, contribution of the wave amplitude (φ) on power loss (Ω^*_{loss}) values is highly dependent on the level of inlet pressure (β); in the lowest β case of 1.01 implementation of higher φ on the upper surface caused Ω^*_{loss} to increase for the complete pad inclination range of $\theta=3°$-$5°$, whereas the role of φ on Ω^*_{loss} counteracts in higher β cases (3.01-5.01) generating lower power loss values for the bearing assembly.

3.4 Bearing load carrying capacity (W^*)

The influences of various φ and θ combinations and wave number (λ) on load carrying ca-

pacity (W^*) for the specific case of $\beta=1.01$ are demonstrated in Fig. 6(a). Computational evaluations point out augmented load data in systems with higher wave amplitudes and with lower pad inclinations; additionally, wave numbers are determined to have a considerable function on the W^* values, such as the increase rates of the load capacity curves are significant in the wave number range of $5 \le \lambda \le 25$. On the other hand, covering the complete wave amplitudes (φ) investigated, fluctuations are recorded in the load values for the wave number range of $\lambda > 25$, in the cavity with $\theta=3°$, where the fluctuations become more identifiable in higher φ cases. Even though the instable nature of the load values is still identifiable for the cavity with $\theta=4°$, the fluctuations are minor when compared with those of the $\theta=3°$ cavity; however further narrowing the lubrication volume to $\theta=5°$ result in continuously increasing, stable style load capacity curves. Numerical computations put forward that above the critical pad inclinations of $\theta_{cr}=3.77°$ ($\beta=1.01$), $\theta_{cr}=4.17°$ ($\beta=3.01$) and $\theta_{cr}=4.22°$ ($\beta=5.01$), the slider bearings, with wavy upper surfaces, are free of fluctuating load values and can safely be assembled to lubrication systems. Instabilities in air journal bearings, due to load fluctuations, were also considered by Su and Lie (2001), who proposed a multi-orifice assembly to create system damping. Designing the slider bearing system, based on optimal load capacity with the criterion of $W^*_{opt}=0.99 W^*_{\lambda=105}$, produces the optimum λ ranges as $10 \to 45$ ($\theta=5°$), $7 \to 11$ ($\theta=4°$) and $5 \to 8$ ($\theta=3°$) in the complete set of wave amplitudes ($\varphi=40 \to 200$ μm) that are taken into consideration. These predictions additionally denote that, the efficiently-applicable wave number ranges are wider in cavities with higher pad inclinations; moreover since the lower and upper limits of these ranges refer to the lowest and highest wave amplitudes of the present work, the design/optimization features of slider bearing systems are highly dependent on the combined effects/interactions of the λ and φ values of the wavy upper-surface definition.

Fig. 6(b) shows the variations of load values with θ and φ for various β cases. It can be seen
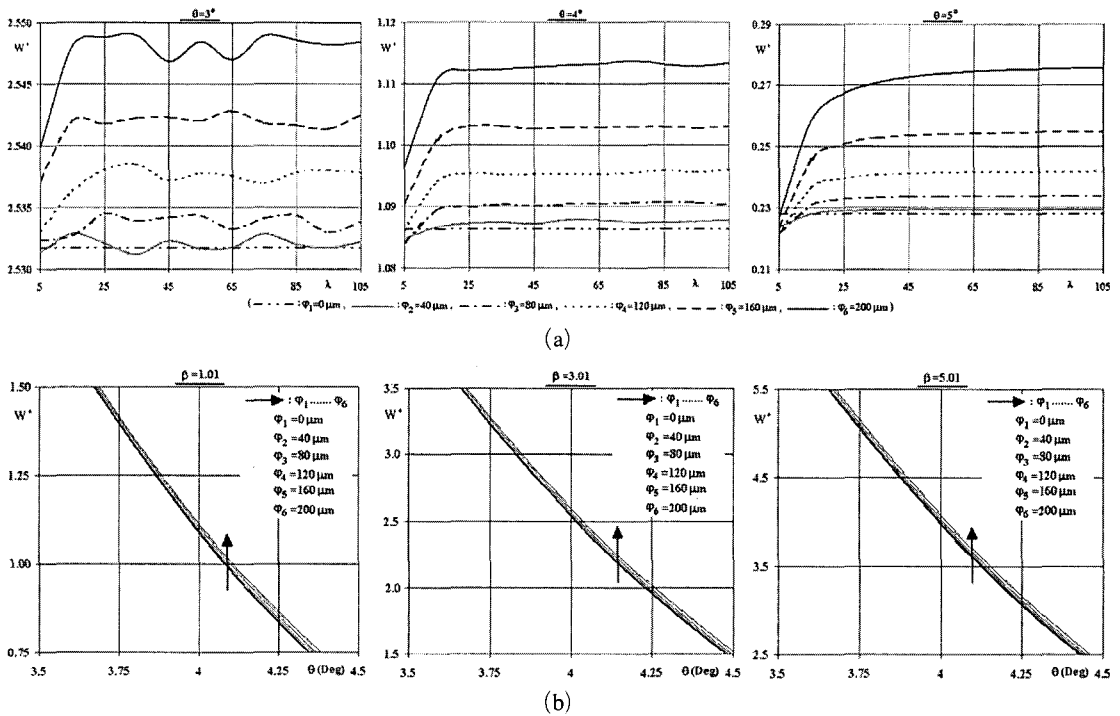
Fig. 6 Combined effects of (a) θ, φ and λ (at $\beta=1.01$) and (b) θ, φ and β (at $\lambda=105$) on bearing load carrying capacity

from the figure that pad inclination has a counter effect on W^*, where associated records were also established by Lin (2001) and van Ostayen et al. (2004) for plain slider bearings. Computations put forward that the influence of pad inclination (θ) on the load values rises as the inlet pressure (β) is increased, such as the W^* values of the $\theta=5°$ pads are 10.81%, 10.18% and 10.02% of the corresponding values of the systems with $\theta=3°$ for β of 1.01, 3.01 and 5.01 respectively. On the other hand, similar with the numerical findings of Su and Lie (2001) on hydrodynamic lubrication of journal bearings and of Karkoub and Elkamel (1997) on gas lubricated rectangular bearings, inlet pressure is determined to have positive effect on the load carrying capacity, where significant augmentations in W^* with higher β are apparent in Fig. 6(b), which can be attributed to the direct relation of inlet pressure, pressure distribution (Eq. (8)) and load data (Eq. (13)). The favorable role of wave amplitude (φ) on load values is clearly displayed both in Figs. 6(a) & 6(b); likewise Rasheed (1998), for cylindrical sliding ele-

ments, and Naduvinamani et al. (2003), for porous rectangular plates, also performed investigations on wave amplitude driven load carrying capacity variations and determined the W^* values to increase with φ. Numerical outputs point out that, for the cavity with $\theta=5°$, the load values of the $\varphi=0$ and $\varphi=200$ μm designs deviate by 20.83%, 13.48% and 11.42% for β of 1.01, 3.01 and 5.01 respectively; whereas the corresponding variations for the pad inclination of $\theta=3°$ are minor and remained in the range of 0.94%–0.66%. These proportions, as a whole, put forward that the impact of wave amplitude on load capacity grows in cases with higher pad inclination and lower inlet pressure. Inspecting Figs. 4(b) & 6(b) simultaneously reveal a close interrelation between the lubricant temperature rise and bearing load capacity data in a wide range of β, θ and φ, but especially for inlet pressure conditions of $\beta \geq$ 3.01 and upper surface designs with $\varphi \leq 120$ μm. Dadouche et al. (2000) also experimentally determined the lubricant temperature values to rise in higher load capacities for hydrodynamic thrust

bearings. The figure pair and the findings indicate that organizing the input parameters for optimal load capacity will also result in significantly augmented lubricant temperature values, which in return may raise the wear rates on the flow surfaces.

4. Conclusions

A parametric study, to characterize the thermodynamic operation scheme of slider bearings, by designing the upper cavity surface in micro-machined wavy-form, is introduced, where the computational method and the findings are applicable for various areas of mechanical applications. Analyzing the system responses for various structural design parameters $(\theta, \varphi$ and $\lambda)$ and boundary conditions (β), made it possible to obtain the individual and combined influences for wide ranges of operation demands. The analysis reveals that the role of wave amplitude on ΔT^* is negligible in the pad inclination ranges of $\theta < 3.77°$, $\theta < 3.91°$ and $\theta < 3.99°$ for β of 1.01, 3.01 and 5.01, whereas the influence of wave amplitude on ΔT^* is determined to drop with inlet pressure. On the other hand, Ω_{loss}^* values are found to augment with higher inlet pressures; the records additionally indicate that the influence of inlet pressure on Ω_{loss}^* is more remarkable in systems with lower pad inclination and wave amplitude. Computational evaluations point out augmented W^* data in systems with higher wave amplitudes and with lower pad inclinations; furthermore, wave numbers are determined to have a considerable function on the W^* values, such as the increase rates of the load capacity curves are significant in the wave number range of 5-25.

References

Ai, X., Cheng, H. S., Hua, D., Moteki, K. and Aoyama, S., 1998, "A Finite Element Analysis of Dynamically Loaded Journal Bearings in Mixed Lubrication," *Tribology Transactions*, Vol. 41, No. 2, pp. 273~281.

Cameron, A., 1981, *Basic Lubrication Theory*, Prentice Hall.

Chapra, S. C. and Canale, R. P., 1990, *Numerical Methods for Engineers*, McGraw Hill.

Cho, I. S., Oh, S. H. and Jung J. Y., 2001, "Lubrication Characteristics Between the Vane and the Rolling Piston in a Rotary Compressor Used for Refrigeration and Air-Conditioning Systems," *KSME International Journal*, Vol. 15, No. 5, pp. 562~568.

Czolczynski, K., 1997, "Stability of the Rotor Supported in Gas Journal Bearings with a Chamber Feeding System," *Wear*, Vol. 210, No. 1~2, pp. 220~236.

Dadouche, A., Fillon, M. and Bligoud, J. C., 2000, "Experiments on Thermal Effects in a Hydrodynamic Thrust Bearing," *Tribology International*, Vol. 33, No. 3~4, pp. 167~174.

Das, N. C., 1998, "A Study of Optimum Load-bearing Capacity for Slider Bearings Lubricated with Couple Stress Fluids in Magnetic Field," *Tribology International*, Vol. 31, No. 7, pp. 393~400.

Hargreaves, D. J. and Elgezawy, A. S., 1998, "A New Model for Combined Couette and Poiseuille Flows in the Transverse Groove of a Plane Inclined Slider Bearing," *Tribology International*, Vol. 31, No. 6, pp. 297~303.

Harsha, S. P., Sandeep, K. and Prakash, R., 2003, "The Effect of Speed of Balanced Rotor on Nonlinear Vibrations Associated with Ball Bearings," *International Journal of Mechanical Sciences*, Vol. 45, No. 4, pp. 725~740.

Honchi, M., Kohira, H. and Matsumoto, M., 2003, "Numerical Simulation of Slider Dynamics During Slider-disk Contact," *Tribology International*, Vol. 36, No. 4~6, pp. 235~240.

Hwang, C. C., Lin, J. R. and Yang, R. F., 1996, "Lubrication of Long Porous Slider Bearings (Use of the Brinkman-extended Darcy Model)," *JSME International Journal (Series B)*, Vol. 39, No. 1, pp. 141~148.

Jeong, H. S. and Kim, H. E., 2004, "On the Instantaneous and Average Piston Friction of Swash Plate Type Hydraulic Axial Piston Machines," *KSME International Journal*, Vol. 18, No. 10, pp. 1700~1711.

Jun, S. C., 2005, "Lubrication Effect of Liquid Nitrogen in Cryogenic Machining Friction on the

Tool-chip Interface," *Journal of Mechanical Science and Technology*, Vol. 19, No. 4, pp. 936~946.

Karkoub, M. and Elkamel, A., 1997, "Modelling Pressure Distribution in a Rectangular Gas Bearing Using Neural Networks," *Tribology International*, Vol. 30, No. 2, pp. 139~150.

Kim, J. K., Kim, H. E., Lee, Y. B., Jung, J. Y. and Oh, S. H., 2005, "Measurement of Fluid Film Thickness on the Valve Plate in Oil Hydraulic Axial Piston Pumps (Part II : Spherical Design Effects)," *Journal of Mechanical Science and Technology*, Vol. 19, No. 2, pp. 655~663.

Kumar, B. V. R, Rao, P. S. and Sinha, P., 2001, "A Numerical Study of Performance of a Slider Bearing with Heat Conduction To the Pad," *Finite Elements in Analysis and Design*, Vol. 37, No. 6~7, pp. 533~547.

Kwan, Y. B. P. and Post, J. B., 2000, "A Tolerancing Procedure for Inherently Compensated, Rectangular Aerostatic Thrust Bearings," *Tribology International*, Vol. 33, No. 8, pp. 581~585.

Lin, J. R., 2001, "Optimal Design of One-dimensional Porous Slider Bearings Using the Brinkman Model," *Tribology International*, Vol. 34, No. 1, pp. 57~64.

Liu, W. K., Xiong, S., Guo, Y., Wang, Q. J., Wang, Y., Yang, Q. and Vaidyanathan, K., 2004, "Finite Element Method for Mixed Elastohydrodynamic Lubrication of Journal-Bearing Systems," *International Journal for Numerical Methods in Engineering*, Vol. 60, No. 10, pp. 1759~1790.

Luong, T. S., Potze, W., Post, J. B., Van Ostayen, R. A. J. and Van Beek, A., 2004, "Numerical and Experimental Analysis of Aerostatic Thrust Bearings with Porous Restrictors," *Tribology International*, Vol. 37, No. 10, pp. 825~832.

Mehenny, D. S. and Taylor, C. M., 2000, "Influence of Circumferential Waviness on Engine Bearing Performance," *Proceedings of the Institution of Mechanical Engineers Part C-Journal of Mechanical Engineering Science*, Vol. 214, No. 1, pp. 51~61.

Na, U. J., 2005, "Fault Tolerant Control of Magnetic Bearings with Force Invariance," *Journal of Mechanical Science and Technology*, Vol. 19, No. 3, pp. 731~742.

Naduvinamani, N.B., Fathima, S.T. and Hiremath, P. S., 2003, "Effect of Surface Roughness on Characteristics of Couple Stress Squeeze Film Between Anisotropic Porous Rectangular Plates," *Fluid Dynamics Research*, Vol. 32, No. 5, pp. 217~231.

Nouri, J. M., Umur, H. and Whitelaw, J. H., 1993, "Flow of Newtonian and Non-Newtonian Fluids in Concentric and Eccentric Annuli," *Journal of Fluid Mechanics*, Vol. 253, pp. 617~641.

Ozalp, A. A. and Ozel, S. A., 2003, "An Interactive Software Package for the Investigation of Hydrodynamic-Slider Bearing-Lubrication," *Computer Applications in Engineering Education*, Vol. 11, No. 3, pp. 103~115.

Pandey, R. K. and Ghosh, M. K., 1998, "A Thermal Analysis of Traction in Elastohydrodynamic Rolling/Sliding Line Contacts," *Wear*, Vol. 216, No. 2, pp. 106~114.

Rasheed, H. E., 1998, "Effect of Surface Waviness on the Hydrodynamic Lubrication of a Plain Cylindrical Sliding Element Bearing," *Wear*, Vol. 223, No. 1~2, pp. 1~6.

Shigley, J. E., 1986, *Mechanical Engineering Design*, McGraw-Hill.

Sottomayor, A., Campos, A. and Seabra, J., 1997, "Traction Coefficient in a Roller—Inner Ring EHD Contact in a Jet Engine Roller Bearing," *Wear*, Vol. 209, No. 1~2, pp. 274~283.

Stokes, M. R. and Symmons, G. R., 1996, "Numerical Optimisation of the Plasto-hydrodynamic Drawing of Narrow Strips," *Journal of Materials Processing Technology*, Vol. 56, No. 1~4, pp. 733~742.

Storteig, E. and White, M. F., 1999, "Dynamic Characteristics of Hydrodynamically Lubricated Fixed-Pad Thrust Bearings," *Wear*, Vol. 232, No. 2, pp. 250~255.

Su, J. C. T. and Lie, K. N., 2001, "Rotation Effects on Hybrid Hydrostatic/hydrodynamic Journal Bearings," *Industrial Lubrication and Tribology*, Vol. 53, No. 6, pp. 261~269.

van Ostayen, R. A. J., Van Beek, A. and Ros, M., 2004, "A Parametric Study of the Hydrosupport," *Tribology International*, Vol. 37, No. 8, pp. 617~625.

Wang, X. L., and Zhu K. Q., "Numerical Analysis of Journal Bearings Lubricated with Micro-

polar Fluids Including Thermal and Cavitating Effects," *Tribology International*, (in Print).

Watanabe, K., Natsume, J., Hashizume, K., Ozasa, T, Noda, T. and Masuda, Y., 2000, "Theoretical Analysis of Bearing Performance of Microgrooved Bearing," *JSAE Review*, Vol. 21, No. 1, pp. 29~33.

Wong, P. L., Xu, H. and Zhang, Z., 1997, "Performance Evaluation of High Pressure Sleeve Seal," *Wear*, Vol. 210, No. 1~2, pp. 104~111.

Yoo, J. G. and Kim, K. W., 1997, "Numerical Analysis of Grease Thermal Elastohydrodynamic Lubrication Problems Using the Herschel-Bulkley Model," *Tribology International*, Vol. 30, No. 6, pp. 401~408.

Yoon, S. J., Kim, M. S. and Choi, D. H., 2002, "Topological Design Sensitivity on the Air Bearing Surface of Head Slider," *KSME International Journal*, Vol. 16, No. 8, pp. 1102~1108.

Appendix :
Non-Dimensional Parameters

Geometric domain is non-dimensionalized by :

$$x^* = \frac{x}{L}, \ y^* = \frac{y}{h_{ex}}, \ h^* = \frac{h}{h_{ex}} \qquad (A1)$$

Velocity terms are non-dimensionalized by :

$$u^* = \frac{u}{V_1}, \ V_u^* = \frac{V_u}{V_1}, \ V_1^* = \frac{V_1}{V_1} = 1 \qquad (A2)$$

Design considerations are non-dimensionalized by :

$$W^* = \frac{W h_{ex}^2}{\mu V_1 L^2}, \ \Omega_{loss}^* = \frac{\Omega_{loss} h_{ex}}{\mu V_1^2 L} \qquad (A3)$$

Primary flow data are non-dimensionalized by :

$$P^* = \frac{P h_{ex}^2}{\mu V_1 L}, \ T^* = \frac{T h_{ex}^2 C_p \rho}{\mu V_1 L} \qquad (A4)$$

Secondary flow data are non-dimensionalized by :

$$q_x^* = \frac{q_x}{h_{ex} V_1}, \ \dot{m}^* = \frac{\dot{m}}{\rho h_{ex} V_1} \qquad (A5)$$